

Precipitation Effects in Mg–Zn Alloys Studied by Positron Annihilation and Hardness Testing

P. HRUŠKA*, J. ČÍŽEK, M. VLČEK, O. MELIKHOVA AND I. PROCHÁZKA

Charles University in Prague, Faculty of Mathematics and Physics

V Holešovičkách 2, 180 00 Praha 8, Czech Republic

In the present work positron annihilation spectroscopy combined with Vickers hardness testing were employed in order to investigate precipitation effects in Mg–Zn alloys. It was found that incoherent precipitates of a metastable Zn-rich phase formed in the samples isochronally annealed above 200 °C cause hardening of the alloy.

DOI: [10.12693/APhysPolA.125.718](https://doi.org/10.12693/APhysPolA.125.718)

PACS: 78.70.Bj, 61.72.J–

1. Introduction

Mg–Zn system is of particular interest in searching for biomedical alloys suitable for biodegradable implants with moderate degradation rate and good mechanical properties since zinc is one of the most abundant elements in the human body [1].

The maximal Zn solubility in Mg is 6.2 wt% (i.e. 2.5 at.%) at 325 °C [2]. At lower temperatures Zn solubility in Mg rapidly decreases. Hence, supersaturated solid solution can be formed by rapid cooling from elevated temperatures. Appropriate subsequent thermal treatment may lead to strengthening due to formation of finally dispersed second phase particles.

In this work positron annihilation spectroscopy (PAS) was employed for investigation of precipitation effects in binary Mg–Zn alloy. Positron lifetime (LT) spectroscopy [3] enables to identify defects and to determine their densities. Coincidence Doppler broadening (CDB) [4] carries information about local chemical environment of defects. Development of mechanical properties was characterized by Vickers hardness (HV) testing.

2. Experimental

Binary Mg–6 wt% Zn alloy (Mg6Zn) was prepared by squeeze casting under protective gas atmosphere (Ar + 1% SF₆). Two sets of samples were investigated: (i) as-cast alloys, (ii) samples subjected to 15 h solution treatment at 320 °C finished by quenching into water at a room temperature. Both samples were then isochronally annealed in steps 20 °C/20 min.

Scanning electron microscopy (SEM) observations were performed on a FEI Phenom microscope.

The HV testing was carried out using a STRUERS Duramin 300 hardness tester. In each HV test a load of 100 g was applied for 10 s.

A ²²Na₂CO₃ positron source (1 MBq) deposited on a 2 μm thick Mylar foil was used. A digital positron lifetime spectrometer [5] with excellent time resolution of

145 ps (FWHM for ²²Na) was employed for LT spectroscopy. The source contribution determined using the well annealed Mg reference sample consists of 2 components with lifetimes of ≈ 368 ps and ≈ 1.5 ns, relative intensities of ≈ 7% and ≈ 1% and representing a contribution of positrons annihilated in the ²²Na₂CO₃ spot and the covering Mylar foil, respectively. The CDB measurements were carried out using a spectrometer described in [6].

3. Results and discussion

3.1. As cast alloy

Figure 1a shows a SEM micrograph of the as-cast Mg6Zn alloy in Z-contrast. Diffuse Zn-enriched bands along grain boundaries separate grain interiors which appear dark due to lower Zn concentration. Thus, in the as-cast sample Zn is not completely dissolved in Mg matrix and excess Zn segregates at grain boundaries.

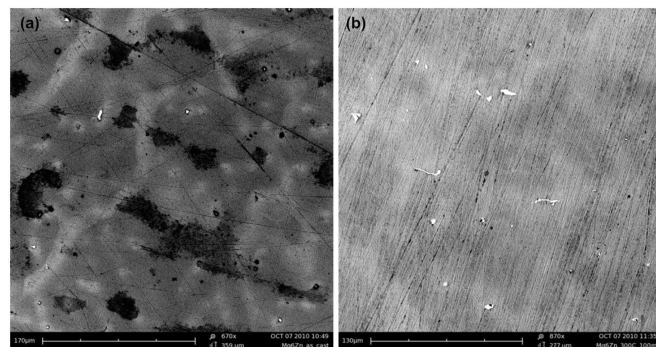


Fig. 1. SEM micrographs using backscattered electrons (Z-contrast): (a) as-cast alloy, (b) sample annealed at 300 °C for 100 min. Let us note that black spots and lines visible in the micrograph are artifacts caused by polishing of sample surface.

Temperature dependence of HV of the as-cast alloy subjected to isochronal annealing is plotted in Fig. 2a. At low annealing temperatures ($T < 100$ °C) HV decreases with increasing temperature most probably due to annealing of dislocations introduced into sub-surface region

*corresponding author; e-mail: peta.hruska.1@gmail.com

of the sample by cutting and polishing. The sample exhibits a single component LT spectrum with lifetime $\tau_1 = 222.8 \pm 0.5$ ps close to the Mg bulk lifetime τ_B [7, 8]. This testifies that the as-cast alloy exhibits very low defect density in the bulk, dislocations induced by cutting and polishing are located in a sub-surface region.

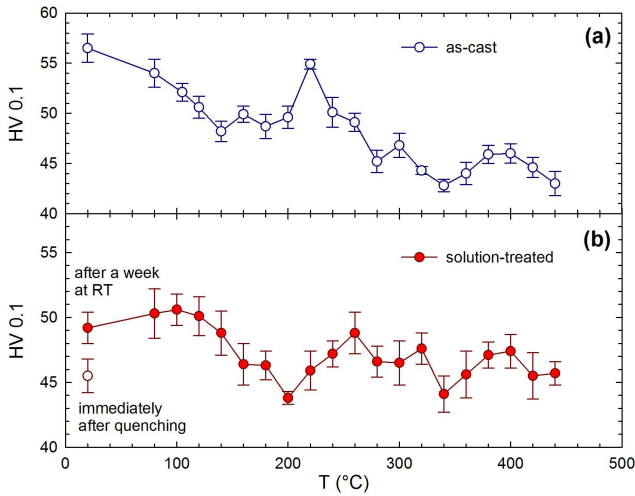


Fig. 2. Temperature dependence of HV (a) as-cast alloy, (b) solution treated alloy.

Further annealing at $T > 180^\circ\text{C}$ leads to an increase of HV which achieves maximum at $T = 220^\circ\text{C}$. This testifies to formation of Zn-rich second phase particles. According to the equilibrium phase diagram of Mg–Zn system [9] formation of MgZn phase can be expected in the alloy studied. However formation of metastable Mg_2Zn_3 and MgZn_2 phases instead of MgZn phase may occur [10]. Our attempt to determine the structure of the second phase by X-ray diffraction was not successful since the volume fraction of second phase is too low. Peak hardening observed at $T = 220^\circ\text{C}$ corresponds to maximum density of the second phase particles. At higher temperatures the second phase precipitates grow in size and their density becomes lower leading to a decrease of HV. Finally, the second phase precipitates are dissolved.

The LT spectra up to $T = 200^\circ\text{C}$ are well fitted by a single component with lifetime τ_1 falling in the range 222–223 ps which is comparable with the Mg bulk lifetime. This testifies that defect density in the alloy is very low. Above 200°C a second component with lifetime $\tau_2 = 256$ ps appeared in LT spectra. The relative intensity I_2 of this component is plotted in Fig. 3 as a function of annealing temperature. I_2 reaches maximum at 220°C , i.e. at the temperature of peak hardening. The lifetime $\tau_2 = 256$ ps agrees well with the lifetime attributed to vacancy-like misfit defects at the interfaces between semicoherent or incoherent precipitates and matrix in Mg alloys [7]. Hence, one can conclude that the component represents a contribution of positrons trapped at vacancy-like misfit defects between Zn-rich second phase precipitates and Mg matrix. Growth and following

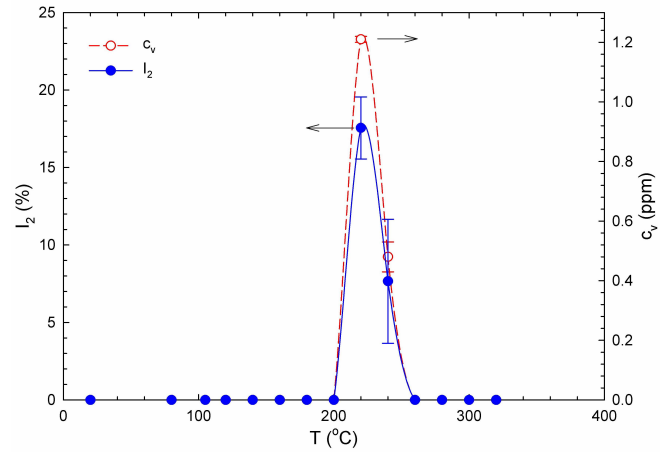


Fig. 3. Temperature dependence of intensity I_2 of positrons trapped at vacancy-like misfit defects in the as-cast alloy (full points); the concentration of vacancy-like misfit defects calculated from LT data using Eq. (1) (open points).

dissolution of the second phase precipitates above 220°C decreases density of misfit defects leading to a decrease of I_2 , see Fig. 3. Finally at $T \geq 260^\circ\text{C}$ I_2 becomes so small that the component cannot be resolved in the LT spectra anymore.

The concentration of misfit defects can be calculated from LT results using the two-state simple trapping model (STM) [11]:

$$c_V = \frac{1}{\nu_V} \frac{I_2}{I_1} \left(\frac{1}{\tau_B} - \frac{1}{\tau_2} \right). \quad (1)$$

For vacancy-like defects in metals specific positron trapping rate ν_V usually falls into the range 10^{14} – 10^{15} s^{-1} . Here we used the lower bound $\nu_V \approx 10^{14} \text{ s}^{-1}$ according to [12]. The concentration of vacancy-like defects determined using Eq. (1) is plotted in Fig. 3 by open circles. Let us note that the quantity [12]:

$$\tau_f = (I_1\tau_1^{-1} + I_2\tau_2^{-1})^{-1} \quad (2)$$

was evaluated and was found to agree well with the Mg bulk lifetime τ_B testifying that STM assumptions are fulfilled.

Precipitation of Zn-rich phase at 220°C was detected also by CDB spectroscopy. Figure 4a shows CDB ratio curves for the as-cast and the isochronally annealed alloy up to 220°C . The CDB ratio curves for pure Zn and Mg reference samples are plotted in Fig. 4b for comparison. All ratio curves presented in Fig. 4a,b are related to well annealed pure Mg. Following the approach developed by Somoza et al. [13] cold rolled pure Mg sample showing saturated positron trapping at dislocations was used to estimate shape of the momentum distribution $n_{\text{Mg},V}$ for positrons trapped at vacancy-like defects and annihilated by Mg electrons. One can see in Fig. 4b that the ratio curve $\rho_{\text{Mg},V}$ is enhanced at low momenta ($p < 5 \times 10^{-3} m_0 c$) and lowered in the high momentum

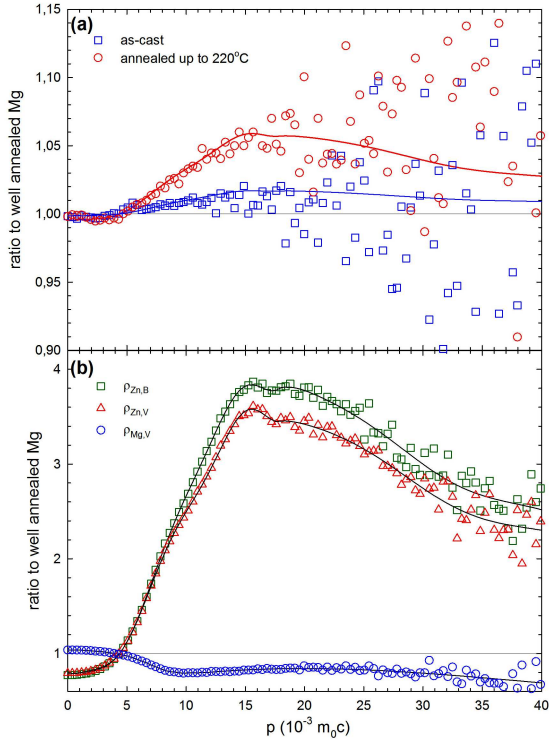


Fig. 4. (a) CDB ratio curves for the as-cast alloy and the sample isochronally annealed up to 220 °C. Solid lines are model functions calculated by Eq. (4); (b) CDB ratio curves for the well defined reference pure Mg and Zn samples. Solid lines are polynomial fits. All CDB ratio curves are related to well annealed Mg.

range due to positron localization at defects. The CDB ratio curves $\rho_{Zn,B}$ and $\rho_{Zn,V}$ for a well annealed Zn (virtually all positrons are annihilated in the free state) and heavily cold rolled Zn (almost all positrons are trapped at vacancy like defects) plotted in Fig. 4b exhibit a broad peak with maximum located at $p \approx 16 \times 10^{-3} m_0 c$ which comes mainly from positrons annihilated by $3d$ Zn electrons. One can see in Fig. 4a that the contribution of positrons annihilated by Zn electrons is more pronounced in the alloy annealed at 220 °C due to precipitation of Zn-rich second phase particles which introduced vacancy-like misfit defects between the precipitates and the matrix. In general, the momentum distribution for Mg6Zn alloy can be expressed as a superposition of the momentum distributions measured in the reference samples

$$n(p) = (1 - F_V) [\xi_{Mg,B} n_{Mg,B}(p) + \xi_{Zn,B} n_{Zn,B}(p)] + F_V [\xi_{Mg,V} n_{Mg,V}(p) + \xi_{Zn,V} n_{Zn,V}(p)]. \quad (3)$$

The ratio curve related to well annealed Mg is obtained by dividing Eq. (3) by $n_{Mg,B}(p)$:

$$\rho(p) = (1 - F_V) [\xi_{Mg,B} + \xi_{Zn,B} \rho_{Zn,B}(p)] + F_V [\xi_{Mg,V} \rho_{Mg,V}(p) + \xi_{Zn,V} \rho_{Zn,V}(p)]. \quad (4)$$

The symbol F_V in Eqs. (3) and (4) is the fraction of positrons annihilated in the trapped state at vacancy-like defects and can be calculated from LT results within STM:

$$F_V = \frac{I_2(\tau_2 - \tau_B)}{\tau_2 - I_2 \tau_B}. \quad (5)$$

The coefficients $\xi_{Mg,B}$ and $\xi_{Zn,B}$ stand for the probability that a free positron is annihilated by Mg or Zn electron, respectively. Similarly the coefficients $\xi_{Mg,V}$ and $\xi_{Zn,V}$ denote the probability that a positron trapped at a vacancy-like defect will be annihilated by Mg and Zn electron, respectively, and characterizes, thereby, chemical environment of vacancy-like defects.

Solid lines plotted in Fig. 4a show fits of ratio curves by Eq. (4) and are in a good agreement with experimental points. For the as-cast alloy $F_V = 0$ (virtually all positrons are annihilated in the free state) and $\xi_{Zn,B} = 0.006 \pm 0.001$. This value is lower than the atomic concentration of Zn in Mg6Zn alloy (2.3 at.%) which confirms that Zn is not completely dissolved in Mg matrix and excess Zn atoms segregate at grain boundaries as observed by SEM, see Fig. 1a. For the alloy annealed up to 220 °C $\xi_{Zn,B} = 0.010 \pm 0.004$ and $\xi_{Zn,V} = 0.50 \pm 0.05$ were obtained from fitting. Hence, annealing caused an increase of $\xi_{Zn,B}$ since a portion of Zn segregated at grain boundaries was dissolved in Mg matrix. Rather high value of $\xi_{Zn,V}$ exceeding significantly the average Zn concentration in the alloy testifies that vacancy-like defects are surrounded by Zn-rich environment. This supports the picture that positrons are trapped at misfit defects between Zn-rich precipitates and Mg matrix.

3.2. Solution treated alloy

A SEM micrograph in Z -contrast of Mg6Zn alloy annealed at 300 °C for 100 min and quenched down to room temperature is shown in Fig. 1b. Since some portion of excess Zn segregated at grain boundaries dissolved in Mg matrix, however slightly brighter regions along grain boundaries are still visible indicating that annealing for 100 min was not long enough for a complete dissolution of Zn in the Mg matrix.

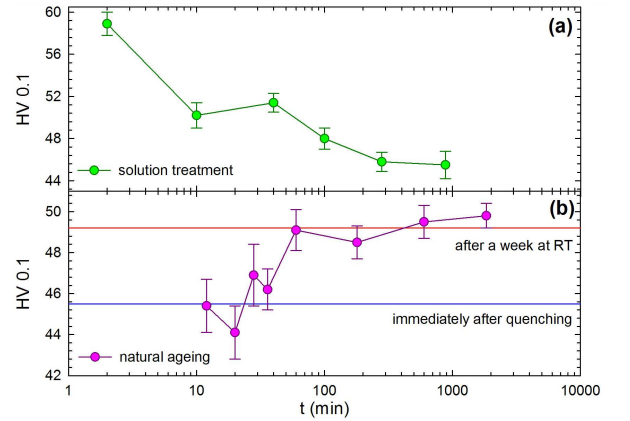


Fig. 5. (a) Development of HV during solution treatment of Mg6Zn at 320 °C; (b) ageing of solution treated alloy at ambient temperature. The bottom line refers to HV of solution treated alloy immediately after quenching. The upper line refers to HV of solution treated alloy after a week at room temperature.

Thus, by long-term solution treatment at 320°C followed by quenching the concentration of Zn in Mg matrix can be enhanced and the distribution of Zn can be made more uniform. Figure 5a shows development of HV during solution treatment at 320°C. HV decreases and finally converges to $HV \approx 46$, i.e. to a value comparable to that measured in the sample isochronally annealed up to 320°C, see Fig. 2a. The alloy solution treated for 15 h was quenched to room temperature and subsequently isochronally annealed in the same regime as the as-cast alloy in order to examine the influence of solution treatment on the precipitation processes. The temperature dependence of HV during isochronal annealing of the solution treated alloy is plotted in Fig. 2b. The hardening above 200°C caused by precipitation of Zn-rich second phase particles is remarkably lower. Moreover, in the solution treated alloy HV firstly increases at low temperatures and reaches maximum at 100°C, which is opposite to the behaviour of the as-cast alloy. Interestingly, the solution treated alloy measured immediately after quenching exhibits $HV = 46 \pm 1$, but when the sample was left at ambient temperature for one week HV increased to 49 ± 1 , see Fig. 2b. This indicates that dissolved Zn atoms agglomerate at ambient temperature into small clusters which are obstacles for movement of dislocations and cause an increase of HV. Clustering of Zn atoms is easier in the solution treated sample, because the mean distance among dissolved Zn atoms is lower and the driving force for clustering is higher due to higher degree of supersaturation.

In order to investigate ageing of Mg6Zn alloy in detail the solution treated sample was kept at ambient temperature and development of HV was examined. Figure 5b shows HV as a function of time of ageing. It is clear that HV increases during ageing and converges to $HV \approx 50$ after ageing for ≈ 15 h. Hence, the increase of HV at low temperatures observed in the solution treated sample in Fig. 2b is most probably due to clustering of dissolved Zn atoms. The same phenomenon is responsible also for lower hardening at $T > 200^\circ\text{C}$ since due to agglomeration of Zn atoms the second phase particles become coarser than in the as-cast alloy.

4. Conclusions

Precipitation effects in Mg6Zn alloy were investigated by PAS combined with HV testing. It was found that Zn-rich second phase particles are formed in the tem-

perature range from 200 to 260°C and cause noticeable hardening of the alloy. Vacancy-like misfit defects are formed at interfaces between the Zn-rich second phase particles and the Mg matrix. In the as-cast alloy only some portion of Zn is dissolved in matrix. Remaining excess Zn atoms are located in bands along grain boundaries. Solution treatment at 320°C enables to dissolve more Zn in the matrix. Solution treated samples exhibit ageing at ambient temperature due to clustering of dissolved Zn atoms. Agglomeration of Zn atoms leads to coarser second phase particles and reduces precipitation hardening in the solution treated samples.

Acknowledgments

This work was supported by the Czech Science Agency (project P108/10/0648) and by the grant SVV-2013-267303. M.V. acknowledges financial support by the Grant Agency of Charles University (project no. 566012).

References

- [1] M. Staiger, A. Pietak, J. Huadmai, G. Dias, *Biomaterials* **27**, 1728 (2006).
- [2] H. Okamoto, *J. Phase Equilibria Diffus.* **15**, 129 (1994).
- [3] P. Hautojärvi, in: *Positrons in Solids*, Ed. P. Hautojärvi, Springer-Verlag, Berlin 1979, p. 1.
- [4] P. Asoka-Kumar, M. Alatalo, V. Ghosh, A. Kruseman, B. Nielsen, K. Lynn, *Phys. Rev. Lett.* **77**, 2097 (1996).
- [5] F. Bečvář, J. Čížek, I. Procházka, J. Janotová, *Nucl. Instrum. Methods Phys. Res. A* **539**, 372 (2005).
- [6] J. Čížek, M. Vlček, I. Procházka, *Nucl. Instrum. Methods Phys. Res. A* **623**, 982 (2010).
- [7] J. Čížek, I. Procházka, B. Smola, I. Stulíková, V. Očenášek, *J. Alloys Comp.* **430**, 92 (2007).
- [8] J.M.C. Robles, E. Ogando, F. Plazaola, *J. Phys., Condens. Matter* **19**, 176222 (2007).
- [9] W. Hume-Rothery, E. Rounsefell, *J. Inst. Met.* **41**, 119 (1929).
- [10] X. Gao, J. Nie, *Scr. Mater.* **56**, 645 (2007).
- [11] R. West, in Ref. [3], p. 89.
- [12] P. Hautojärvi, C. Corbel, in: *Proc. Int. School of Physics "Enrico Fermi", Course CXXV*, Eds. A. Dupasquier, A. Mills, IOS Press, Varenna 1995, 491.
- [13] A. Somoza, M. Petkov, K. Lynn, A. Dupasquier, *Phys. Rev. B* **65**, 094107 (2002).